INTERNATIONAL SOCIETY FOR
SOIL MECHANICS AND
GEOTECHNICAL ENGINEERING

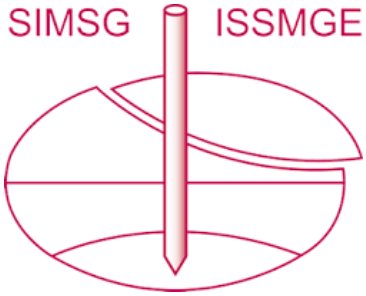

This paper was downloaded from the Online Library of the International Society for Soil Mechanics and Geotechnical Engineering (ISSMGE). The library is available here:

https://www.issmge.org/publications/online-library

This is an open-access database that archives thousands of papers published under the Auspices of the ISSMGE and maintained by the Innovation and Development Committee of ISSMGE.

The paper was published in the proceedings of the 7th International Conference on Earthquake Geotechnical Engineering and was edited by Francesco Silvestri, Nicola Moraci and Susanna Antonielli. The conference was held in Rome, Italy, 17 – 20 June 2019.

Earthquake Geotechnical Engineering for Protection and Development of Environment and Constructions – Silvestri & Moraci (Eds)
© 2019 Associazione Geotecnica Italiana, Rome, Italy, ISBN 978-0-367-14328-2

Simple guidelines for the seismic design of yielding semi-gravity cantilever walls

R. Conti & V.G. Caputo
Università di Roma Niccolò Cusano, Rome, Italy

ABSTRACT: This paper presents a numerical and theoretical investigation on the physical mechanisms that control the dynamic behaviour of yielding cantilever walls and, in turn, affect their seismic design. To this end, an extensive numerical study is carried out, taking into account different wall geometries, soil properties and input earthquakes. Numerical outcomes show that the maximum soil thrust on the stem and the maximum bending moment are always in phase and occur when the inertia forces are directed away from the backfill. Moreover, when a plastic mechanism is triggered, the actual average acceleration of the soil-wall system can differ significantly from the free-field one, by restricting also the maximum possible inertia force. Based on numerical results and theoretical considerations, a simple pseudostatic limit equilibrium/analysis model is presented, providing a good prediction of both the critical acceleration of the wall and its maximum internal forces.

1 INTRODUCTION

The seismic design of yielding cantilever walls is usually carried out with a pseudostatic approach, *i.e.* converting the seismic acceleration acting on the system to an equivalent constant pseudostatic coefficient and computing the resulting soil thrust using either limit equilibrium methods or limit analysis. Despite the simplifying assumptions, the pseudostatic approach has been proven to provide valuable information on the seismic behaviour of yielding retaining structures, where the onset of plastic mechanisms within the soil-structure system makes the dynamic interaction problem a strength-driven rather than a deformability-driven problem (Conti *et al.*, 2012, 2013, 2014).

Figure 1(a) shows the typical layout for a cantilever wall, retaining a cohesionless backfill and resting on a cohesive-frictional soil. Figure 1(b) shows the forces acting on the soil-wall system under the horizontal ($a_h=k_hg$) and vertical ($a_v=k_vg$) pseudostatic accelerations, the latter being usually neglected as of minor relevance in the seismic design of gravity walls. Both the dynamic active soil thrust acting on the vertical plane AV, S_{AV}, its inclination on the horizontal, δ_S, and the inclination of the two failure surfaces, ω_α and ω_β, were derived by Kloukinas & Mylonakis (2011) and Evangelista *et al.* (2010) in the realm of a rigorous stress plasticity theory.

The external stability of the system against the possible onset of plastic mechanisms (geotechnical design) must be assessed under the outlined system of external forces, giving rise to an inclined and eccentric resultant at the foundation level. In this context, the critical acceleration of the wall, a_c, is defined as the one corresponding to which a plastic mechanism is activated within the soil-structure system and the wall starts to experience permanent displacements. Specifically, $a_c = \min(a_{y,SLID}, a_{y,QLIM})$, where $a_{y,SLID}$ and $a_{y,QLIM}$ are the pseudostatic yield accelerations corresponding to which the strength of the system is fully mobilised under a pure sliding mechanism (Richards & Elms, 1979) and a bearing capacity failure (Conti, 2018), respectively.

When dealing with the internal stability of the vertical stem (structural design), the soil thrust effectively acting on its back (S_E) must be taken into account, resulting from the dynamic interaction between the soil volume above the heel and the wall (Figure 1(c)). Table 1 reports two possible approximate solutions for $S_{E,h}$. In the first case (S1), it is assumed that no

Table 1. Approximate theoretical solutions for the horizontal force acting on the vertical stem.

Solution	$S_{E,h}$	M_{max}	$\sigma_h(z)$
$S1(k_h)$	$S^{KM}_{AE,h}(k_h) + k_h W_s$	$S^{KM}_{AE,h}(k_h) \cdot H/3 + k_h\left(W_{w,stem} + W_s\right) \cdot H/2$	$K^{KM}_{AE,h} \cdot \gamma z + k_h \cdot \gamma d$
$S2(k_h)$	$S^{MO}_{AE,h}(k_h)$	$S^{MO}_{AE,h}(k_h) \cdot H/3 + k_h W_{w,stem} \cdot H/2$	$K^{MO}_{AE,h} \cdot \gamma z$

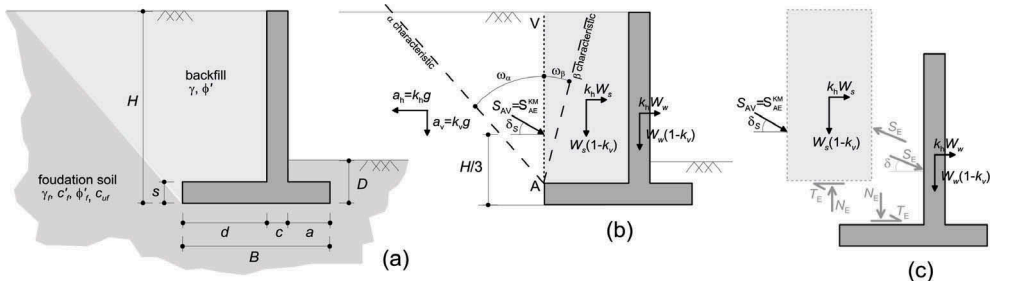

Figure 1. Cantilever walls: (a) typical layout; (b) system of pseudostatic external forces; (c) assessment of the internal stability.

shear stresses develop at the contact between the heel and the soil above it ($T_E = 0$), and hence the soil thrust S_{AV} and the inertia forces $k_h W_s$ are entirely transferred to the vertical stem. The second solution (S2), instead, assumes that the soil volume above the heel is in active limit state conditions and that the presence of the horizontal stem does not alter the resulting soil thrust. In this condition, S_E can be computed using the Mononobe-Okabe (MO) theory.

Within this general framework, two issues are still under debate: (i) the applicability of the Mononobe-Okabe (MO) theory in computing the dynamic soil thrust and (ii) the possible phase shift between the maximum value of the soil thrust and the inertia forces into the wall-soil system. While many authors agree that the dynamic pressure behind the wall increases linearly with depth (Mikola *et al.*, 2016), centrifuge data have shown that the MO method can lead to a significant over prediction of the soil thrust acting on the vertical stem, particularly for high values of free-field accelerations (Koseki *et al.*, 2003). As far as the second issue is concerned, Kloukinas *et al.* (2015) and Al Atik & Sitar (2010) suggested the possible occurrence of phase shift between maximum (active) inertia forces into the system, maximum soil dynamic thrust and maximum bending moments, but providing different and controversial interpretations of the actual physical phenomenon.

Based on the results of an extensive numerical and theoretical work (Conti & Caputo, 2018), this paper aims at identifying the relevant factors affecting the seismic behaviour of yielding cantilever walls and providing suggestions for their seismic design.

2 NUMERICAL MODEL

2.1 *Problem layout*

Figure 2 shows the problem layouts analysed in this work. Three different geometries were considered for the wall (W1, W2, W3), varying only in the length of the toe. Two different soil deposits were chosen, including a cohesionless (soil #2) and a cohesive (soil #3) soil layer immediately beneath the foundation, with drained (D) and undrained (UD) behaviour respectively.

2.2 *Numerical model*

Plane-strain analyses were carried out on a pair of cantilever walls, retaining an ideal 16 m wide and 5 m deep rectangular excavation, using the finite difference code FLAC v.5 (Itasca, 2005).

Table 2. Ground motion parameters of the input earthquakes.

Earthquake	PGA	PGV	PGD	f_d	$T_{5\text{-}95}$
	[g]	[m/s]	[m]	[Hz]	[s]
Northridge - USA (1994)	0.582	0.514	0.108	1.28	9.0
Loma Prieta - USA (1989)	0.372	0.443	0.183	0.72	10.4
Kobe - Japan (1995)	0.329	0.281	0.116	0.58	11.8
Imperial Valley - USA (1979)	0.330	0.307	0.162	7.15	8.4
Hollister - Usa (1961)	0.194	0.120	0.044	0.88	14.6
Chi Chi - Taiwan (1999)	0.214	0.198	0.180	0.74	11.7
Friuli - Italy (1976)	0.324	0.222	0.042	3.78	4.2
Kocaeli - Turkey (1999)	0.337	0.609	0.502	0.78	14.7

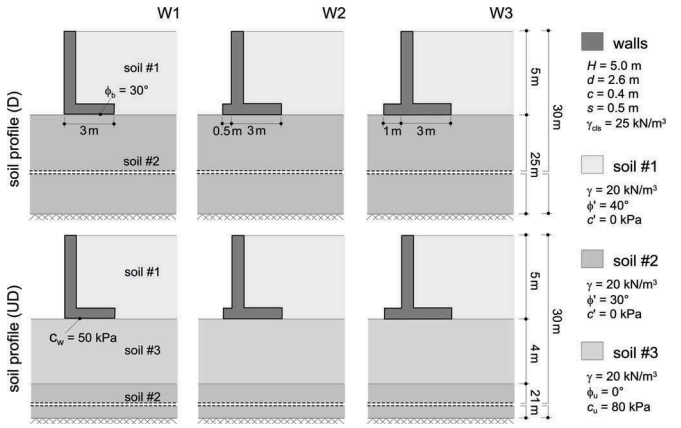

Figure 2. Problem layouts considered in the numerical study.

The retaining walls were modelled as elastic beams (ρ = 2.55 Mg/m^3, E = 40 GPa, ν = 0.15), connected to the grid nodes using elastic-perfectly plastic interfaces.

The soil was modelled as an elastic-perfectly plastic material with a Mohr-Coulomb failure criterion and a non-associated flow rule, with zero dilatancy. During the dynamic stage, a non-linear and dissipative behaviour was introduced for stress paths within the yield surface through a hysteretic model available in the FLAC's library, which basically extends to general strain conditions the one-dimensional unloading-reloading Masing's rules (1926) (see *e.g.*: Conti *et al.*, 2014).

2.3 *Procedure of analysis*

After the initial static stage, dynamic analyses were carried out. The selected acceleration time histories were applied to the bottom nodes of the grid, together with a zero velocity in the vertical direction, while standard periodic constraints were applied to the lateral boundaries of the grid. Eight input signals were chosen to represent a significant range of dominant frequencies and peak accelerations (see Table 2). Moreover, simple wavelet excitations were applied, with a nominal frequency of 0.8 Hz, scaled at maximum accelerations ranging from 0.05 g to 0.35 g.

Summarizing, a total of 78 dynamic analyses were carried out, taking into account different wall geometries (W1, W2, W3), different soil conditions (D, UD) and different seismic inputs. More details about the numerical model and procedure are given in Conti & Caputo (2018). In the following, accelerations are positive rightwards and the horizontal displacements of the walls are positive if away from the backfill. Points N_{TOP}, N_{MID}, N_{BOT} and N_{ff} – respectively at the top, mid-height and bottom of the wall, and in free-field conditions – will be considered in the discussion of results.

3 NUMERICAL RESULTS

3.1 *Wavelet input signals*

In order to clarify some aspects concerning the dynamic behaviour of yielding cantilever walls, we will first concentrate on the simple case of a wavelet input acceleration (a_{max} = 0.15 g). The wall W1 will be used as reference, overlying both the D and UD soil profile, to highlight possible differences between the sliding (W1-UD, $a_c = a_{y,SLID}$) and bearing (W1-D, $a_c = a_{y,QLIM}$) failure modes.

Figure 3 shows, for the right wall, the time histories of: (a, b) free-field and wall absolute horizontal accelerations; and (c, d) horizontal displacements of the wall. The absolute accelerations of the wall coincide with the free-field one as long as the critical value, a_c, is not exceeded. For larger values of the free-field acceleration, the wall starts to move, by either a combination of rotation and sliding (D) or pure sliding (UD). During these time intervals, the accelerations at the top and at the bottom of the stem can vary, if the wall rotates, but the acceleration at mid height of the stem – representative of the average acceleration of the soil-wall system (Conti & Caputo, 2018) – remains approximately constant and equal to a_c. Moreover, walls accelerations can be out of phase with respect to the free-field ones, mostly depending on the extent of the ongoing permanent displacement.

Figure 4 shows, for the right wall, the time histories of: (a, b) free-field and wall absolute horizontal accelerations; (c, d) the total horizontal force computed in the soil elements immediately behind the vertical stem, $S_{E,h}$; and (e, f) the bending moment at the base of the stem.

Figure 4 also reports the horizontal soil thrust (c, d) and the maximum bending moment (e, f) predicted by the two approximate solutions S1(k_h=k_c) and S2(k_h=k_c) (critical condition). $S_{E,h}$

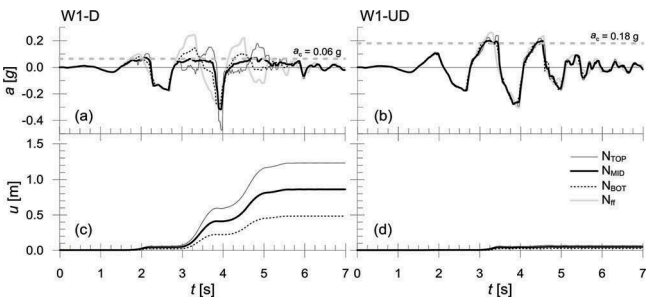

Figure 3. Right Wall W1, soil profile D and UD. Time histories of: (a, b) horizontal free-field and wall accelerations; (c, d) wall displacements.

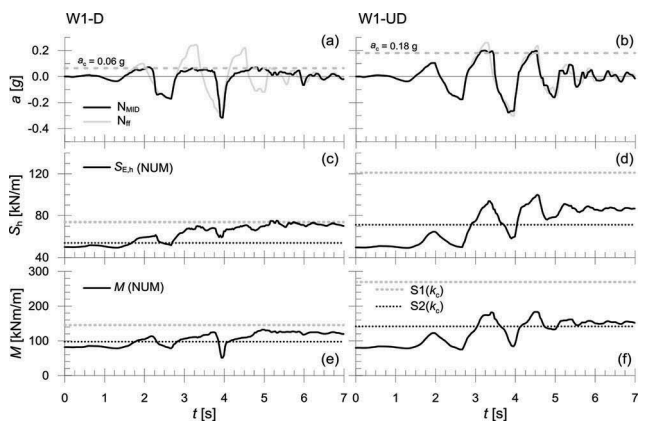

Figure 4. Right Wall W1, soil profile D and UD. Time histories of: (a, b) horizontal free-field and wall accelerations; (c, d) horizontal soil thrust behind the stem; (e, f) bending moment at the base of the stem.

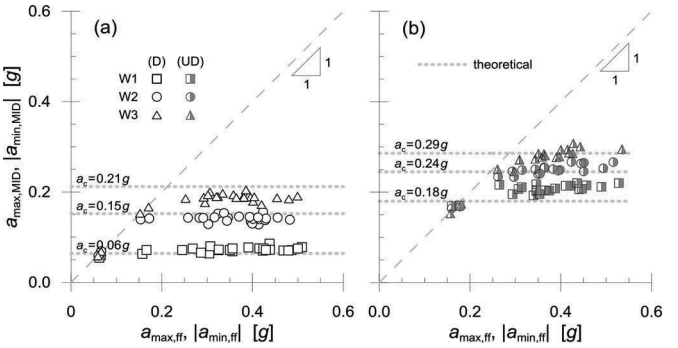

Figure 5. Maximum horizontal accelerations of the wall (N_{MID}) as a function of the maximum free-field acceleration (N_{ff}): (a) soil profile D and (b) soil profile UD.

reaches its maximum under positive (rightwards) accelerations, that is when the inertia forces into the soil-wall system are directed away from the backfill. This result, in apparent contradiction of what observed for gravity retaining walls (Conti *et al.*, 2013), stems from the fact that S_E, as being an internal force between the wall and the backfill, depends on the masses W_w/g and W_s/g. It follows that, when cantilever walls are concerned (W_w significantly smaller than W_s), S_E is always maximised when the backfill is "pushing" towards the wall (rightwards accelerations). The maximum value of $S_{E,h}$ depends on the amount of shear stress transferred through the internal heel, T_E, which is related to the shear deformations at the contact between the heel and the soil above it and which could hardly be predicted within a perfect plasticity framework. Moving to the bending moments, their maximum value, M_{max}, occurs together with the maximum soil thrust behind the stem. Comparing the numerical results with the approximate solutions S1(k_c) and S2(k_c), in terms of both horizontal soil thrust and bending moment, it is clear that S1(k_c) provides always a physical upper bound for their maxim values.

3.2 *Real input earthquakes*

The dynamic response of cantilever walls during real earthquakes is discussed in terms of synthetic parameters, usually adopted as performance indicators for the system.

Figure 5 reports the maximum acceleration computed at mid height of the stem (N_{MID}) against the maximum free-field acceleration (N_{ff}), for the drained (a) and the undrained (b) analyses, together with the theoretical values of the critical acceleration. Maximum rightwards ($a_{max,MID}$, $a_{max,ff}$) and leftwards ($|a_{min,MID}|$, $|a_{min,ff}|$) accelerations are considered for the right and the left wall respectively. As expected, once the critical threshold is attained - *i.e.* as soon as a plastic mechanism develops within the soil-wall system - the absolute acceleration of the system remains approximately constant, starting to deviate from the free-field excitation. Moreover, the theoretical predictions of a_c are in good agreement with the numerical results.

Figure 6 shows the maximum normalised bending moment, $M_{max}/\gamma H^3$, as a function of the maximum free-field acceleration. The approximate solutions S1(k_h), S1(k_c) and S2(k_h) are also plotted for comparison. For a given layout, the maximum bending moment can increase even for $a_{max,ff} > a_c$, even though the absolute acceleration of the system remains constant, due to an internal redistribution of stresses leading to a reduction of T_E. Nonetheless, the solution S1 (k_c), corresponding to $T_E = 0$, always defines the upper bound for M_{max}. Moreover, as long as this limiting condition is not achieved, the solution S2($k_h = a_{max,ff}/g$) provides a reasonable estimate of the maximum internal forces in the stem, with a maximum relative scatter of about 20%, in terms of bending moment, with respect to the numerical values.

4 DISCUSSION OF RESULTS AND SUGGESTIONS FOR DESIGN

Based on the numerical results, the following conclusions can be drawn regarding the forces acting on the wall and the accelerations in the soil-wall system:

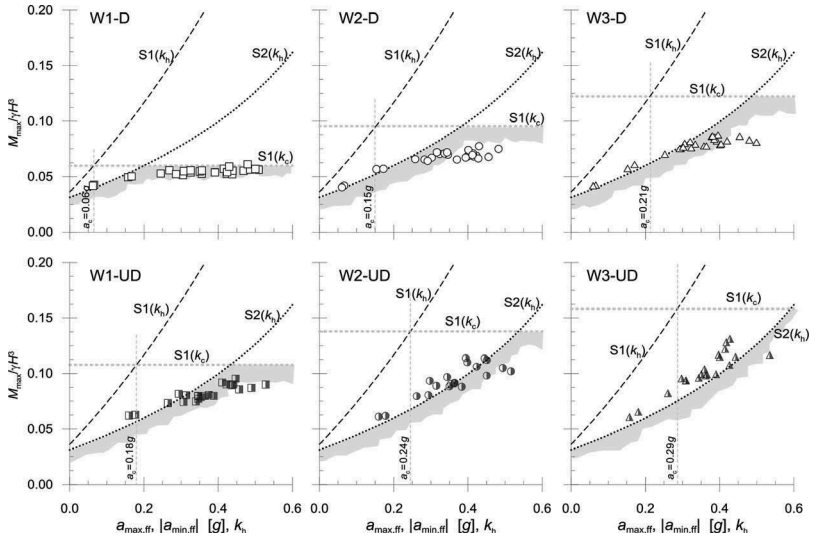

Figure 6. FDM analyses: maximum bending moment as a function of maximum free-field acceleration.

a. During a dynamic event, the maximum values of $S_{E,h}$ and of the structural bending moment are always in phase and occur when the inertia forces into the system are directed away from the backfill.
b. Possible phase shifts can occur between free-field and wall accelerations, when the wall undergoes permanent displacements. Moreover, the actual average acceleration of the soil-wall system can differ significantly from the free-field one, its physical upper bound corresponding to the critical value a_c.
c. Up to the critical condition ($k_h \leq k_c$, where $k_h = a_{max,ff}/g$), the MO pseudostatic solution provides a good estimate of the active soil thrust acting on the vertical stem.
d. As soon as a plastic mechanism develops within the soil-wall system ($k_h > k_c$), the average absolute acceleration of the system remains constant. As a consequence, also the maximum inertia force that the system can ever experience during an earthquake is bounded by its critical value. Moreover, the pseudostatic solution S1(k_c) (corresponding to $T_E = 0$) must define the upper bound for $S_{Eh,max}$ and M_{max}, *i.e.* the maximum internal forces that the wall would ever experience during an earthquake.
e. The maximum internal forces in the wall ($S_{Eh,max}$, M_{max}) can increase even for $k_h > k_c$, even though the absolute acceleration of the system remains constant, due to an internal redistribution of stresses leading to a reduction of T_E. This behaviour cannot be predicted within a perfect plasticity framework, as it depends on the amounts of shear deformations at the contact between the heel and the soil above it. However, from a practical point of view, the solution S2(k_h) provides a reasonable estimate of the maximum internal forces in the stem until the limiting condition S1(k_c) is not achieved.

A further remark refers to the possible contribution coming from the cohesion of the foundation soil to the critical mechanism of the wall, both in drained (cohesive-frictional soils) and undrained (purely cohesive soils) conditions. As a matter of fact, while the bearing capacity mechanism is usually the critical one for a cohesionless foundation soil, the sliding mechanism is also possibly critical in the case of cohesive-frictional soils. As an example, Figure 7 shows the yield acceleration, k_y, as a function of the ratio R_d/E_d between the design values of the static resisting and driving forces, for both the sliding and the bearing failure mechanism ($B = 2/3H$; $a = B/3$; $s = c = H/12$). As evident, soil's cohesion can affect significantly the critical mechanism, and this implication could be relevant for relatively dense or bonded foundation soils.

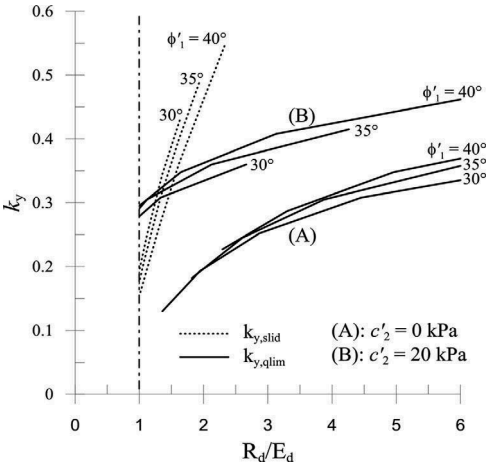

Figure 7. Dependence of k_y on the static ratio R_d/E_d for the sliding and bearing failure mechanisms, for different values of φ'_1,φ'_2 and c'_2 ($B = 2/3H$; $a = B/3$; $s = c = H/12$).

Based on the above results, a simple three-step procedure for the structural design of cantilever retaining walls can be defined, taking into account, though approximately, the possible contribution of the horizontal stem to the overall dynamic equilibrium. As summarised in Figure 8:

a. compute the critical acceleration of the wall;
b. use S1(k_c) to compute the maximum internal forces that the wall could ever experience during an earthquake;
c. for a given design earthquake, corresponding to which $k_h = a_{max,ff}/g$, use S2(k_h) to compute the internal forces in the wall, as long as S2(k_h) < S1(k_c), otherwise use S1(k_c).

As far as the geotechnical design is concerned, the concept of an admissible wall displacement has been widely accepted within the performance-based seismic design philosophy (Pender, 2018). However, the possibility of admitting wall tilting, related to a temporary attainment of the bearing resistance, is still a controversial issue. Indeed, many provisions and codes of practice still recommend to design the wall ensuring an adequate safety margin with respect to a bearing failure of the foundation and assuming the sliding mechanism as the critical one. The rationale behind it is twofold: (1) an excessive wall tilting could induce a sudden

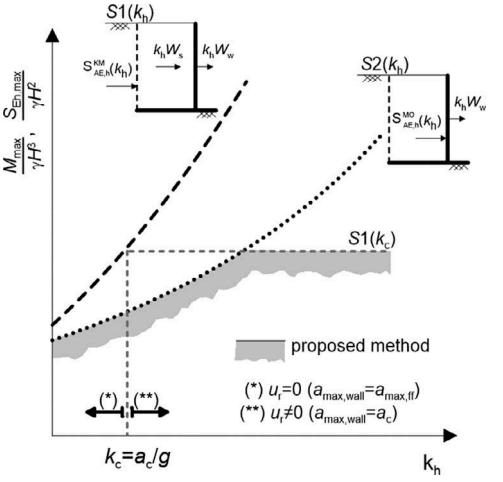

Figure 8. Pseudostatic method for the structural design of yielding cantilever walls.

collapse of the wall by overturning; (2) no reliable procedures are available to accommodate a mixed sliding-rotational failure mode within the well-established Newmark's approach.

With this respect, a rational seismic design of gravity/cantilever walls should contemplate the possible activation of both mechanisms, instead of excluding a priori the expected rotation. As a matter of fact, the temporary mobilisation of the soil shear resistance beneath the foundation would not lead to a fragile failure of the system, provided that an excessive wall tilting is prevented. This is a fundamental difference with respect to a pure overturning mechanism, which is indeed a fragile mechanism by nature. On the other hand, further research is required to develop reliable (and simple) theoretical models, capable of handling combined tilting and sliding failure modes as, in this case, a direct application of the Newmark's sliding block procedure can lead to a significant under-prediction of the final displacement (Conti & Caputo, 2018).

5 CONCLUSIONS

The numerical results presented in this paper shed light on the physical mechanisms affecting the seismic behaviour of yielding cantilever walls. It has been shown that the critical acceleration is the key ingredient for their seismic design, controlling both the maximum structural internal forces and the final displacement. A simple pseudostatic model was proposed for the structural design of cantilever walls, based on limit equilibrium/analysis methods. However, further research is required to develop reliable models for the prediction of wall permanent displacements, capable of handling combined tilting and sliding failure modes.

REFERENCES

Al Atik, L., Sitar, N. 2010. Seismic earth pressures on cantilever retaining structures. *J. Geotech. Geoenviron. Eng*., 136(10),1324-1333.

Conti, R., Madabhushi, S.P.G. and Viggiani, G.M.B 2012. On the behaviour of flexible retaining walls under seismic actions. *Géotechnique*, 62(12),1081-1094.

Conti, R., Viggiani, G.M.B., Cavallo, S. 2013. A two-rigid block model for sliding gravity retaining walls. *Soil Dyn. Earth. Eng*., 55, 33-43.

Conti, R., Viggiani, G.M.B, Burali d'Arezzo, F. 2014. Some remarks on the seismic behaviour of embedded cantilevered retaining walls. *Géotechnique*, 64(1),40-50.

Conti, R. 2018. Simplified formulas for the seismic bearing capacity of shallow strip foundations. *Soil Dyn. Earth. Eng*., 104, 64-74.

Conti, R. & Caputo, G. 2018. A numerical and theoretical study on the seismic behaviour of yielding cantilever walls. *Géotechnique*, DOI: 10.1680/jgeot.17.P.033

Evangelista, A., Scotto di Santolo, A., Simonelli, A.L. 2010. Evaluation of pseudostatic active earth pressure coefficient of cantilever retaining walls. *Soil Dyn. Earth. Eng*., 30, 1119-1128.

Itasca 2005. FLAC Fast Lagrangian Analysis of Continua v. 5.0. User's Manual.

Kloukinas, P., Mylonakis, G. 2011. Rankine solution for seismic earth pressures on L-shaped retaining walls. 5ICEGE. Santiago Chile.

Kloukinas, P., Scotto di Santolo, A., Penna, A., Dietz, M., Evangelista, A., Simonelli, A.L., Taylor, C., Mylonakis, G. 2015. Investigation of seismic response of cantilever retaining walls: Limit analysis vs shaking table testing. *Soil Dyn. Earth. Eng*., 77, 432-445.

Koseki, J., Tatsuoka, F., Watanabe, K., Tateyama, M., Kojima, K., Munaf, Y. 2003. Model tests of seismic stability of several types of soil retaining walls. Reinforced soil engineering: Advances in research and practice. Ling, H. I., Leshchinsky, D. and Tatsuoka, F. eds., New York, 317-358.

Masing G. Eigenspannungen und Verfertigung bim Messing. In: Proceedings of the 2nd international congress on applied mechanics, Zurich; 1926.

Mikola, R.G., Candia, G., Sitar, N. 2016. Seismic Earth Pressures on Retaining Structures and Basement Walls in Cohesionless Soils. *J. Geotech. Geoenviron. Eng*., 142(10), 04016047.

Pender, M. J. 2018. Foundation design for gravity retaining walls under earthquake. *Proceedings of the institutions of Civil Engineers: Geotechnical Engineering*, DOI: 10.1680/jgeen.17.00233

Richards, R., Elms, D.G. 1979. Seismic behaviour of gravity retaining walls. *J. Geotech. Eng. Div*., ASCE, 105(4),449-464.